"REVIEWED"

NUMERICAL SIMULATION OF CLOUD SEEDING USING A THREE-DIMENSIONAL CLOUD MODEL

Richard D. Farley, Phuong Nguyen, and Harold D. Orville
Institute of Atmospheric Sciences
South Dakota School of Mines and Technology
501 E. St. Joseph Street
Rapid City, South Dakota 57701-3995

Abstract. This preliminary study is concerned with the numerical modeling of cloud seeding effects in three dimensions for the deep convective cloud case of 19 July 1981 from the CCOPE field experiment. The observed cloud was relatively isolated and grew rapidly to about 11 km height. An extensive anvil was produced. For the first time in our 3D modeling efforts, a silver iodide (AgI) seeding agent is introduced into a three-dimensional cloud model. Ice and precipitation formation occurs 2 min earlier in the seeded case. Maximum mixing ratios show only slight increases (about 5% for graupel/hail) compared to the unseeded case. Domain totals of graupel/hail and rain indicate a more pronounced seeding effect, consistent with surface rainfall estimates of a 20% increase for the seeded case. For the 3D case in this study, 10% of the AgI remains unactivated, caught in a dead zone of virtually no net transport to the southeast of the cloud around 4 km AGL. The use of an inert agent, sulfur hexafluoride, for comparison purposes helps to illustrate the region of activated AgI.

1. INTRODUCTION

Extensive work has been done by our modeling group and others using two-dimensional, time-dependent (2DTD) cloud models to simulate cloud seeding experiments (Hsie *et al.*, 1980; Kopp *et al.*, 1983; Orville and Chen, 1982; Orville *et al.*, 1984; Farley, 1987). Results of these and other studies have shown that the seeded clouds exhibit earlier development of precipitation, relatively slight dynamic enhancement of the updraft, sometimes dramatic differences in cloud life history, and normally precipitation increases of a few to several tens of percent in moderate size convective cells. The results have emphasized the strong interactions of microphysics and dynamics in the model clouds such that precipitation decreases result sometimes. The hypothesis normally tested is the microphysical one of increasing the precipitation efficiency of a cloud.

The code for the cloud seeding methods has been added to the Clark and associates 3D cloud model in addition to the ice microphysics of the Institute of Atmospheric Sciences (IAS) cloud models. This preliminary report shows the results of seeding a moderate size convective cell using a 3D cloud model.

The atmospheric conditions used as initial conditions for the model are taken from a CCOPE case (19 July 1981) that has been studied extensively in WMO workshops and results published in several papers (e.g., Helsdon and Farley, 1987; Dye *et al.*, 1986). The atmospheric conditions (Fig. 1) produce an active cell that first reaches cumulonimbus proportion, produces one lightning flash, some rain and small hail, and an extensive anvil. Updrafts of 10 - 15 m s^{-1} were observed; the simulations show over 20 m s^{-1} maximum updrafts.

The general results for this 3D case are that ice and precipitation formation occur 2 min earlier in the seeded case than in the unseeded case. Maximum mixing ratios show only slight increases (about 5% for graupel/hail) compared to the unseeded case. Domain totals of graupel/hail and rain indicate a more pronounced seeding effect, consistent with surface rainfall estimates of a 20% increase for the seeded case. For this case, 10% of the AgI remains unactivated, caught in a dead zone of virtually no net transport to the southeast of the cloud around 4 km AGL.

A few of the results that lead to these conclusions are given in the following pages.

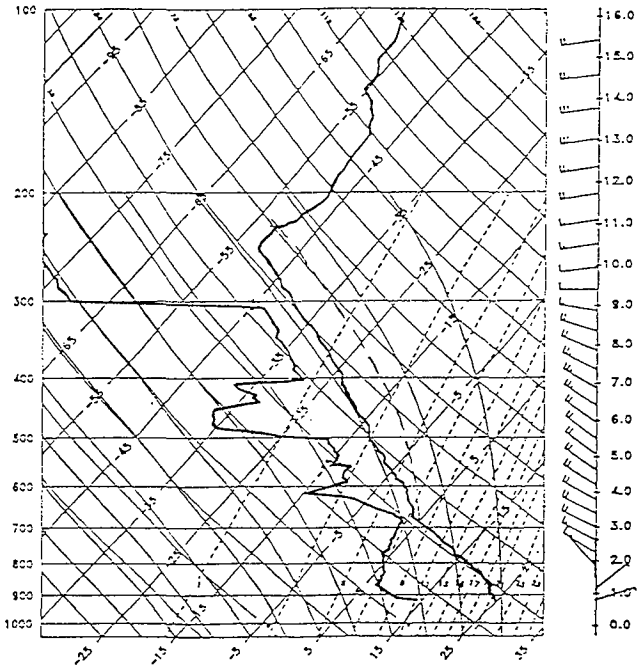

Fig. 1: A representative sounding taken at 1440 MDT (Mountain Daylight time) from Miles City on July 19, 1981.

2. BRIEF THREE-DIMENSIONAL MODEL DESCRIPTION

The three-dimensional cloud model used in this study was developed by Clark and associates (Clark, 1977, 1979, 1982; Clark and Farley, 1984). The model uses the deep anelastic equations of Ogura and Phillips (1962) and originally employed bulk water microphysics similar to Kessler (1969) for cloud water and rain mixing ratios. Recently, this model has been modified to use the bulk water parameterization scheme of Lin *et al.* (1983) with additional microphysical refinements. These are graupel/hail formation via snow (of a certain critical size) accreting supercooled cloud water as explained by Farley *et al.* (1989) and a parameterization of the rime-splintering ice multiplication scheme as described in Aleksić *et al.* (1989). Sub-grid scale turbulence is parameterized according to the first-order theory of Smagorinsky (1963) and Lilly (1962). The eddy mixing coefficients are functions of the flow field and the local Richardson number, so that both wind shear and thermal stability determine the magnitude of the coefficients. Open boundary conditions are used at the side boundaries as described in Clark (1979). The domain of the model is 20 km x 20 km x 15 km with grid intervals of 400 m x 400 m x 250 m in the x, y, z-directions. Time steps of 6 s are used.

For this study, the seeding agent field has been added to the 3D model. This development allows for the seeding agent to be an inert tracer such as sulfur hexaflouride (SF_6) or an artificial ice nucleation agent such as silver iodide (AgI), or dry ice (CO_2). The treatment of AgI follows the scheme outlined in Hsie *et al.* (1980) and that for dry ice is handled as described in Kopp *et al.* (1983). In this paper, only the SF_6 and AgI treatments will be discussed.

Farley *et al.* (1992) discuss simulations of the 19 July 1981 CCOPE case using single and nested model configurations of the 3D model used in this study, concentrating on comparisons to observations. The current set of 3D simulations differ from those in Farley *et al.* (1992) in that the subcloud moisture has been reduced slightly, the direction of the low-level winds has been modified, and a weaker perturbation has been used to initiate the convection. All of these changes were made to produce a less active cloud, especially in the early stages, to create a larger time window for seeding. Consequently, comparison of these results with the particular observations from 19 July 1981 is not pertinent.

3. THREE-DIMENSIONAL MODEL RESULTS

3.1 General Appearance of the Cloud Field

Figure 2 shows three-dimensional depictions of the cloud life cycle viewed from the northeast (NE) at 4-min intervals starting at 8-min simulation time. The perspectives were produced by plotting the surface of the combined cloud water and cloud ice field at $q_{cw} + q_{ci} = 0.1$ g kg^{-1}. Initial cloud formation was at 6 min after initiation. The cloud grows quite rapidly, and the upper portion extends toward the south and east by 16 min. At 20 min, the formation of an anvil becomes apparent. The anvil top develops into an irregular, rough shape and begins to break apart after 30 min. The cloud grows further toward the north and east by 32 min with the low-level support still concentrated along the west side. The turrets appear to be tallest at this time. The lower level of the cloud expands and by 36 min, new growth generated by the outflow shows up. Additional weak new growth can be seen at later times.

3.2 Silver Iodide Evolution

Figure 3 displays 3D depictions of the evolution of the AgI field viewed from the northeast. The numbers on the left corner are the simulation time in minutes. These 3D depictions display the 10^{-3} μg kg^{-1} surface of the silver iodide (AgI) field. The AgI was introduced at the cloud top at 8 min with a maximum value of 3.5 E-10 g g^{-1}. The pattern of seeding gives a total of approximately 47 g of AgI spread over nearly 3.5 km in the horizontal (elongated in the x-direction) and over about

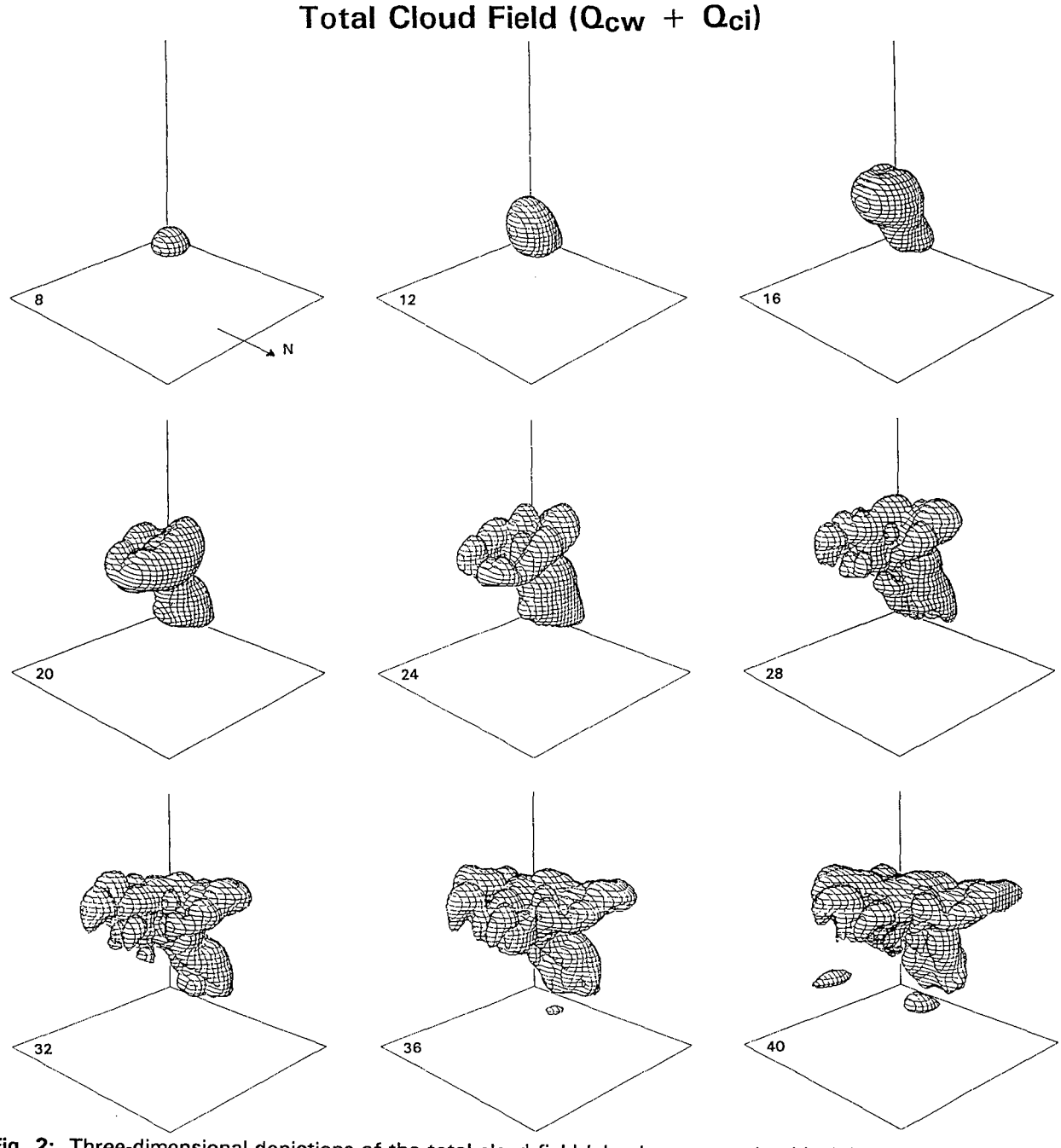

Fig. 2: Three-dimensional depictions of the total cloud field (cloud water + cloud ice) for the unseeded case viewed from the northeast. The 0.1 g kg^{-1} surface is indicated in these panels. The numbers on the left corner are the simulation time in minutes.

1 km in the vertical. The AgI spreads out towards the south and east directions. At 12 min, it forms a wicket shape as the unactivated AgI is draped over the southeast quadrant of the cloud. Also at 12 min, much of the AgI has been used up in the upper portion of the cloud. This can be seen quite clearly at 14 min. The AgI is continually activated as long as it stays above -5°C. By 20 min, only a small amount of AgI at lower levels remains. At 22 min, that portion of the AgI field which has not been activated has been diffused to values less than the plotting threshold of 10^{-3} μg kg^{-1}.

Figure 4a shows the X-Z and X-Y cross sections of the AgI field at 10 and 12 min. The panels at 10 min show some of the AgI has been used up and some has been transported to the east. The portion which is advected to the southeast quadrant is not activated since it is transported outside the cloud and quickly descends to a region where the temperature is warmer than -5°C (the activation temperature for AgI). The unactivated AgI transported to the southeast is also clearly shown in the lower right panel. Most of the AgI to the west has been activated by 14 and 16 min,

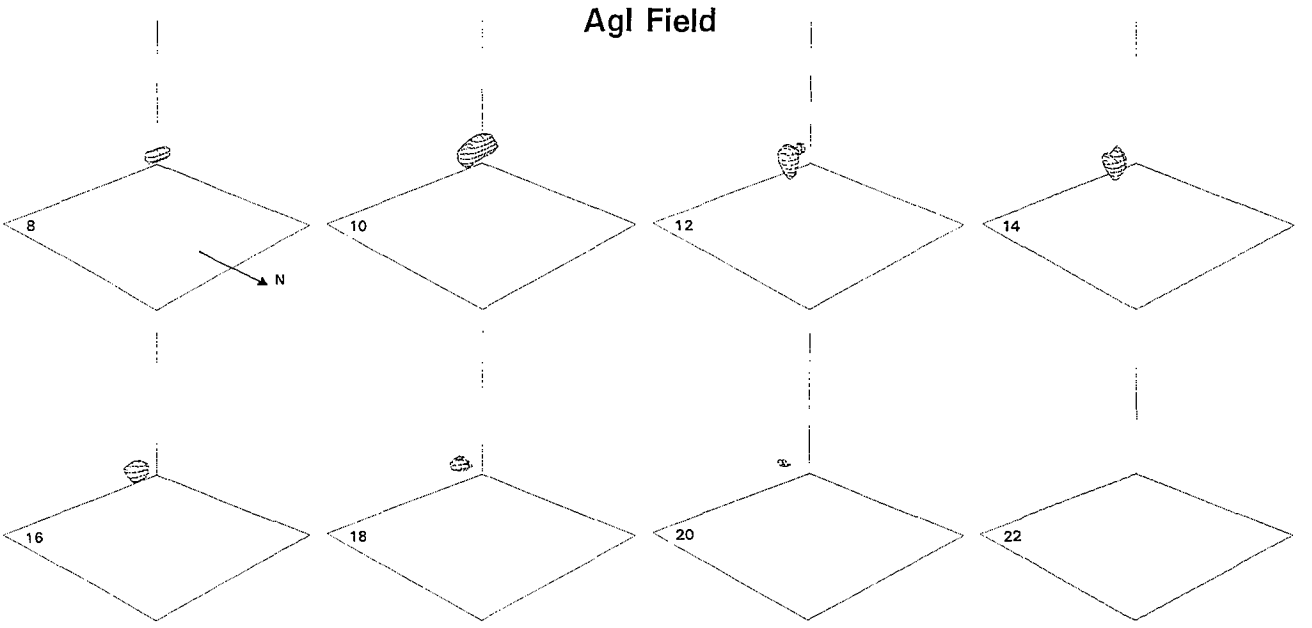

Fig. 3: The silver iodide (AgI) evolution viewed from the northeast. The numbers on the left corner are the simulation time in minutes .

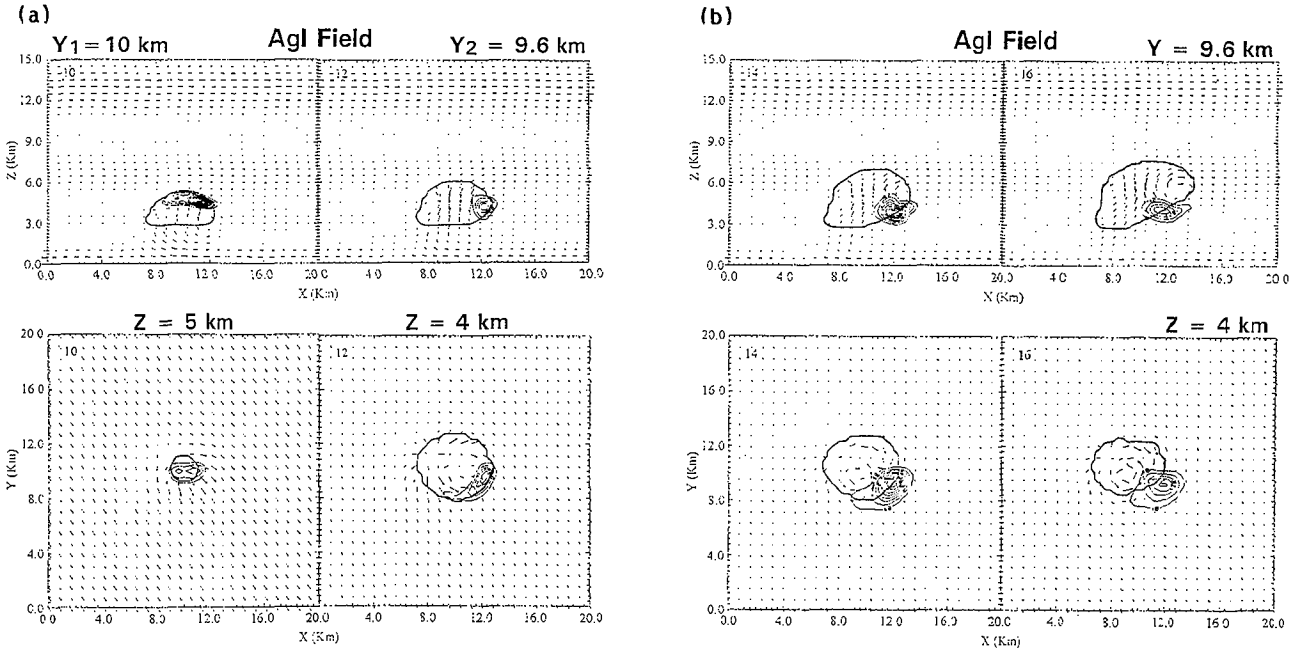

Fig. 4: (a) Top two panels are the vertical X-Z cross sections of the AgI field at y = 10 km at 10 min and y = 9.6 km at 12 min. The bottom two panels are horizontal X-Y cross sections at z = 5 km (left) and z = 4 km (right). The contour interval is 0.0025 μg kg^{-1} for 10 min and 0.001 μg kg^{-1} for 12 min. The arrows show the two dimensional representation of the wind appropriate for the particular plane. The bold solid line indicates the cloud outline. (b) Top two panels are X-Z cross sections of the AgI field at y = 9.6 km at 14 and 16 min. The bottom two panels are X-Y cross sections at z = 4 km at the same times. The contour interval is 0.0004 μg kg^{-1}.

as shown in Fig. 4b. The remaining AgI is concentrated in a "dead zone" to the southeast as can be seen quite clearly in this figure. There is little net transport of the AgI out of this dead zone as the AgI is slowly diffused.

3.3 Inert Tracer Field (SF_6) Evolution

An inert tracer, sulfur hexafluoride (SF_6), is simulated to illustrate where the AgI would have diffused if it had not been activated. Figure 5 illustrates the evolution of the inert tracer field (SF_6) in 3D depictions viewed from the northeast. The number in the left corner of each panel indicates the simulation times in minutes. These 3D depictions display the 10^{-3} μg kg^{-1} surface of the inert tracer (SF_6) field. The SF_6 is introduced at the cloud top at 8 min in the same manner that AgI was applied. By 12 min, the SF_6 extends to the south and east and begins to form a wicket shape. At 16 min, the diffusion of the SF_6 is becoming evident with the SF_6 plume spreading out towards the south and east. Diffusion continues until the field is broken into isolated pockets in excess of the plotting threshold, first evident at 22 min. By 26 min, the figure shows that the top part of the SF_6 field has diffused below the plotting threshold and only an isolated pocket of concentrated SF_6 is evident. By 32 min, the entire SF_6 field has been diffused below the threshold value.

Figure 6a,b shows the evolution of the SF_6 field in X-Z and X-Y cross sections from 10 to 16 min. From this figure, it is easy to see the transport of the SF_6 toward the south and east and downward at 12 min. Figure 6b shows the continuing tendency of SF_6 to be concentrated in the southeast quadrant at around 4 km AGL. Referring back to Fig. 4a, we see that the unactivated AgI tends to be concentrated in the same region. By comparing Fig. 6 with Fig. 4, we also get a good picture of where the AgI is being activated, namely at all elevations above approximately 5 km.

We next look at the development of some of the microphysical fields in the unseeded and seeded cases. The cloud ice and snow fields are not shown here but are analyzed in the thesis by Nguyen (1993).

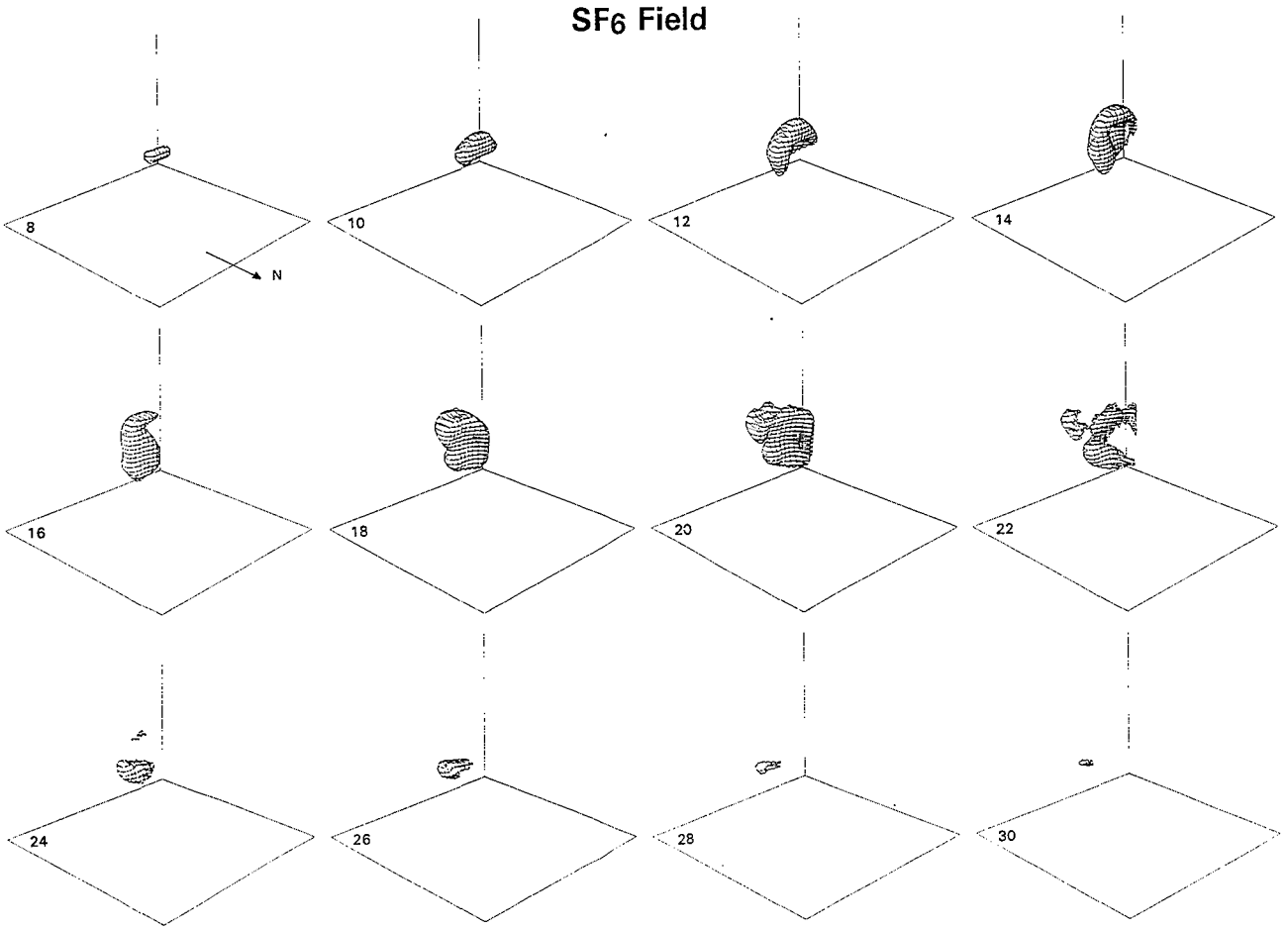

Fig. 5: The inert tracer (SF_6) evolution viewed from the northeast. The numbers in the left corner are the simulation time in minutes.

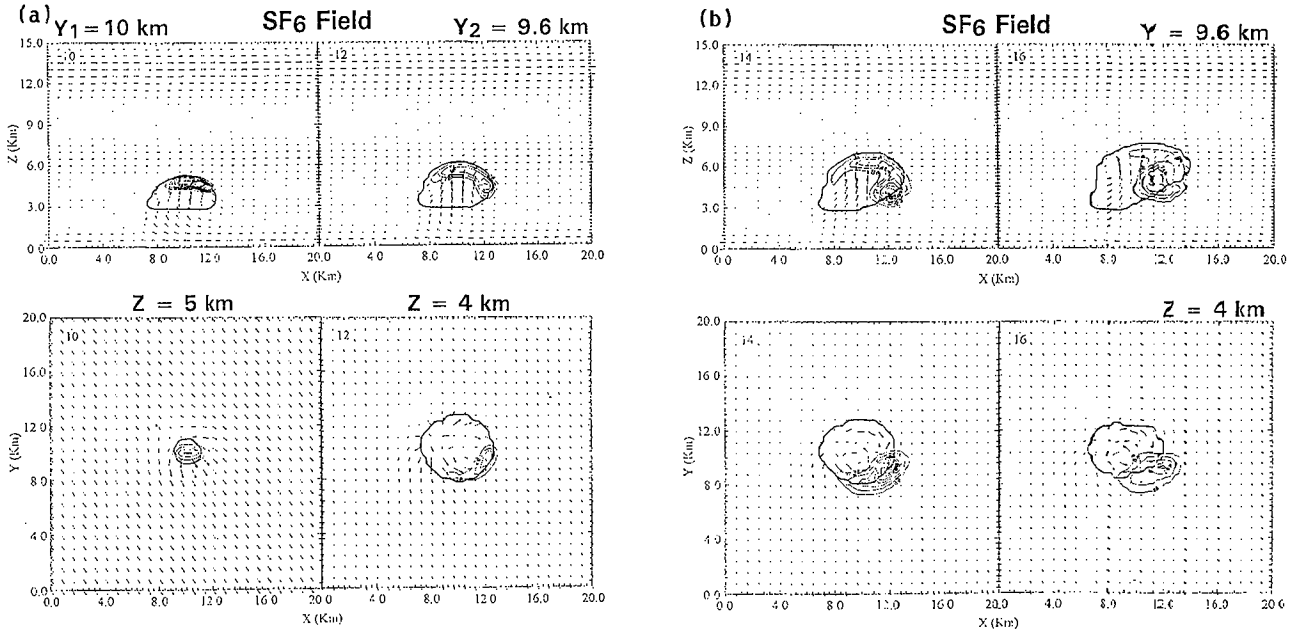

Fig. 6: (a) Top two panels are X-Z cross sections of the SF_6 field at y = 10 km at 10 min and y = 9.6 km at 12 min. The bottom panels are X-Y cross sections at z = 5 km at 10 min and z = 4 km at 12 min. The contour interval is 0.005 μg kg^{-1} at 10 min and 0.002 μg kg^{-1} at 12 min. The arrows show the two-dimensional representation of the wind appropriate for the particular plane. (b) Top panels are X-Z cross sections of the SF_6 field at y =9.6 km at 14 and 16 min. The bottom panels are X-Y cross sections at z = 4 km at the same times. The contour interval is 0.0008 μg kg^{-1} for all panels.

3.4 Development of the Unseeded Graupel/Hail Field

At 16 min, graupel/hail has formed through riming of the snow particles. This initial graupel/hail formation occurs in the updraft core between 6 and 7 km above ground level (AGL). The maximum value of graupel/hail at this time is 1.3 E-4 g kg^{-1}. By 18 min, the maximum amount increases to 0.47 g kg^{-1}. At 20 min, the graupel/hail field is located close to the updraft core, mainly from around 6 to 9 km above the ground level. Two minutes later (22 min), portions of the graupel/hail field have been carried downstream and begin descending toward the ground, and by 24 min, the graupel/hail particles begin to fall out of the cloud on the downshear side of the updraft. This is illustrated in Fig. 7a. The X-Z cross sections (upper panels) of this figure clearly indicate three hail cores. A strong development can be seen in the core to the left (west) which is still within the updraft region. The other two cores are weakening. As the graupel/hail falls below the 0°C isotherm, which is located at 3.25 km AGL, melting begins to occur, leading to the formation of rain.

Figure 7b shows the later development of the three cores at 26 and 28 min. The top panels show that the middle and the right cores of graupel/hail have been melting at lower levels. The decrease which is seen on the east side of the cores in the bottom panels indicates that most of the hail in these cores has fallen out. The maximum value of graupel/hail is recorded at 26 min (2.32 g kg^{-1}). It decreases slowly until 38 min and then increases again. This is due to a new cell to the northwest which has grown tall enough for significant graupel/hail development.

3.5 Development of the Seeded Graupel/Hail Field

Graupel/hail has first formed at 14 min in the seeded case (2 min earlier compared to the unseeded case). The maximum value of graupel/hail at this time is 1.2 E-3 g kg^{-1}. It increases two orders of magnitude by 16 min. By 18 min, the maximum amount increases to 1.2 g kg^{-1}. This is one order of magnitude larger compared to the unseeded case at the same time. By 22 min, the development of the three graupel/hail cores is clearly shown (Fig. 8a). Greater amounts of graupel/hail are indicated at these times compared to the unseeded case shown in Fig. 7a. It is noted that the graupel/hail particles in this case begin to fall out around 22 min. This is also the time when the first significant rain can be seen for the seeded case. The maximum graupel/hail mixing ratio is 2.6 g kg^{-1} occurring at 24 min (2 min earlier than the unseeded case maximum).

Figure 8b shows the later evolution of the same cross sections at 26 and 28 min. At these times, the graupel/hail field for the seeded case is very similar to the unseeded case results shown in

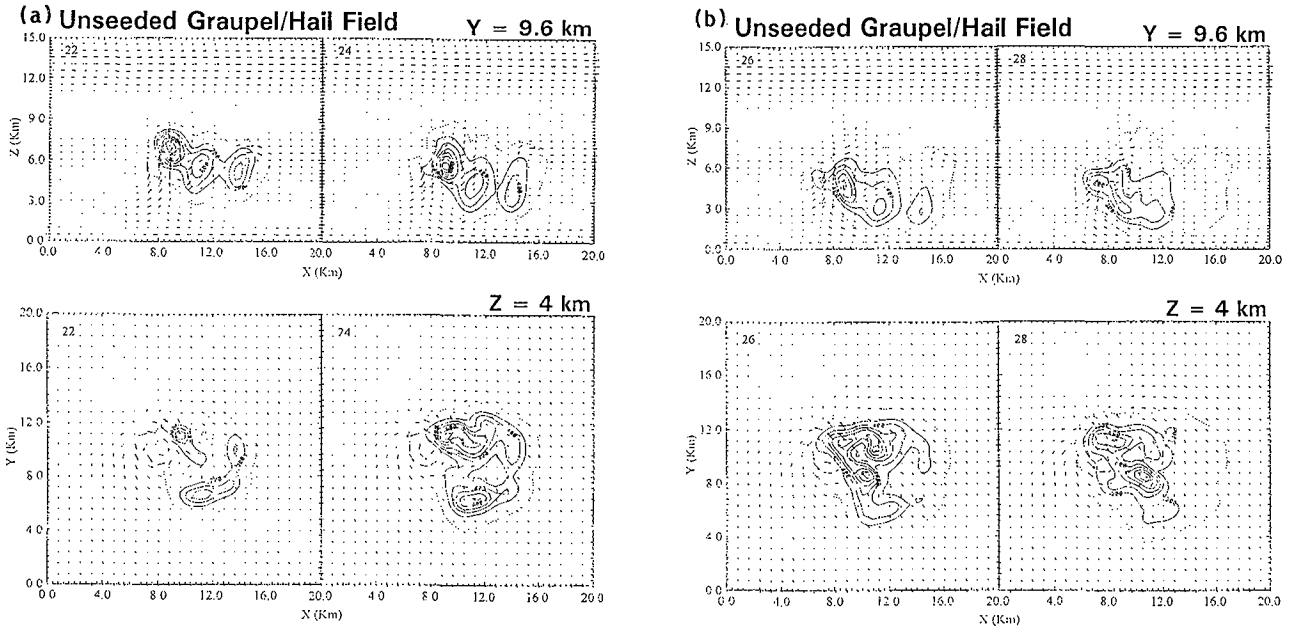

Fig. 7: (a) Top two panels are X-Z cross sections of the graupel/hail field at y = 9.6 km at 22 and 24 min for the unseeded case. The bottom two panels are X-Y cross section at z = 4 km for the same times. The contour interval is 0.2 g kg^{-1}. The arrows shows the two-dimensional representation of the wind appropriate for that particular plane. (b) As in Fig. 7(a), but at 26 and 28 min.

Fig. 7b. The maximum graupel/hail mixing ratio for the seeded case decreases until 38 min, and then increases slowly up to 1.4 g kg^{-1} by 44 min.

3.6 Development of the Unseeded Rain Field

Figure 9 shows the development of the rain field, which forms from the melting of graupel/hail, beginning around 24 min. The maximum mixing ratio at this time is 0.19 g kg^{-1}. It is obvious that the development of these two rain cores is the result of the melting process operating on the lower portions of the center and the right cores of the graupel field shown in Fig. 7a at 24 min. Both cores are growing rapidly and approaching the ground by 28 min. The left core reaches the

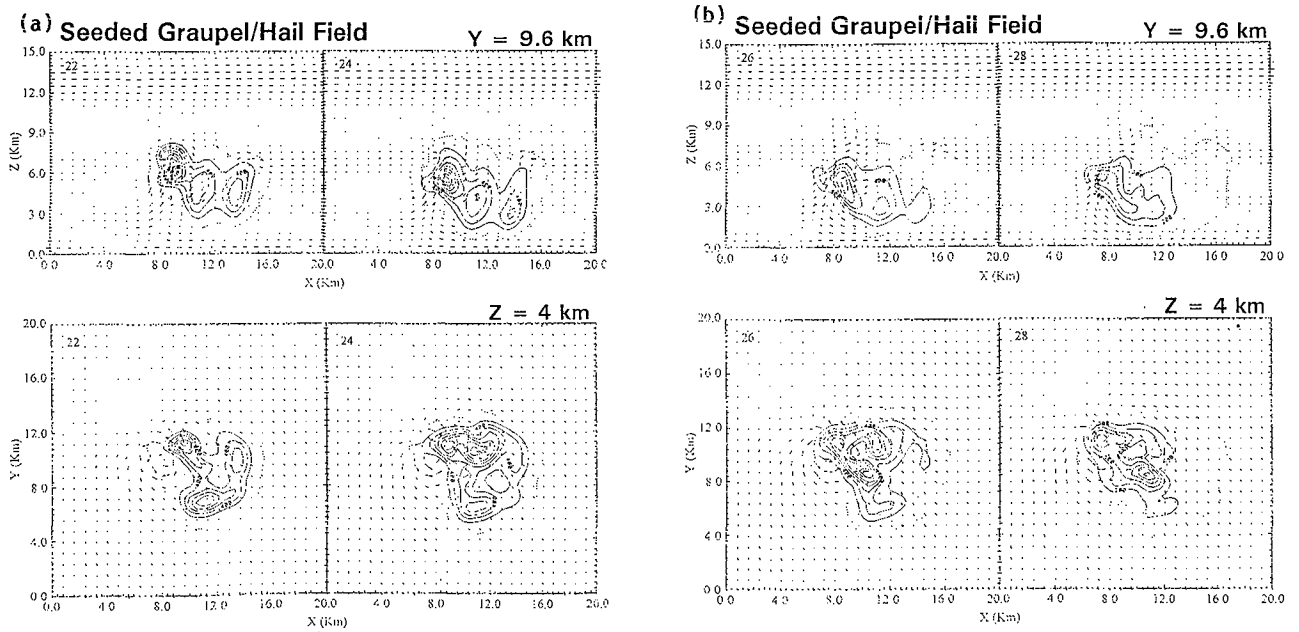

Fig. 8: (a) Top two panels are X-Z cross sections of the graupel/hail field at y = 9.6 km at 22 and 24 min for the seeded case. The bottom panels are X-Y cross sections at z = 4 km for the same times. The contour interval is 0.2 g kg^{-1} in all panels. The arrows show the two-dimensional representation of the wind appropriate for that particular plane. (b) As in Fig. 8(a), but at 26 and 28 min.

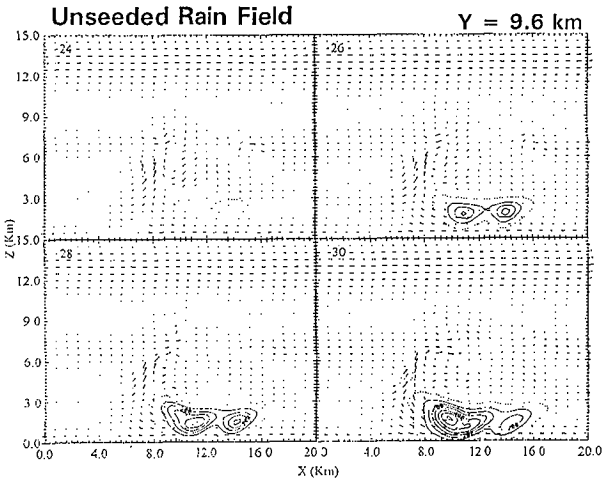

Fig. 9: X-Z cross sections of the rain field at y = 9.6 km from 24 to 30 min for the unseeded case. The contour interval is 0.1g kg^{-1} in all panels. The arrows show the wind in the X-Z plane.

ground by 30 min. The maximum mixing ratio at this time is around 1.0 g kg^{-1}.

Figure 10 shows horizontal cross sections of the rain field at the surface from 30 to 36 min. At 30 min, two rain cores are clearly defined. These two cores merge by 34 min and continue to intensify until 36 min. The rain core to the northwest is the dominant surface rainfall producer of the simulation. The maximum rain mixing ratio of 1.15 g kg^{-1} is recorded at this time. After 36 min, the values decrease slightly until the end of the period of consideration (44 min).

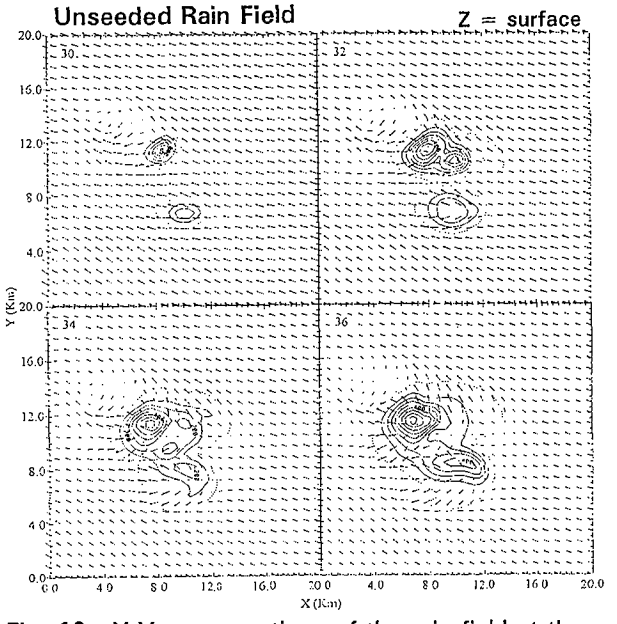

Fig. 10: X-Y cross sections of the rain field at the model surface from 30 to 36 min for the unseeded case. The contour interval is 0.1 g kg^{-1} in all panels. The arrows show the wind in the X-Y plane.

3.7 Development of the Seeded Rain Field

At 22 min, the first significant amounts of rain are indicated in the seeded case. The maximum rain mixing ratio at this time is 0.12 g kg^{-1}. Figure 11 shows X-Z cross sections of the rain field from 24 to 30 min for the seeded case. At 24 min, two rain cores are clearly defined and appear to be much stronger than those shown in Fig. 9 for the unseeded case. Both rain cores develop until 26 min. By 28 min, the left (western) rain core continues to grow while the right (eastern) rain core has begun to dissipate. Both rain cores reach the ground at this time with a maximum rain mixing ratio of 1.0 g kg^{-1}. The maximum rain mixing ratio for the seeded case is 1.2 g kg^{-1} at 30 min. Similar to the unseeded case, the formation of these two cores in the seeded rain field is the result of the graupel/hail melting process which shows up in Fig. 8 at 24 min. The maximum value slowly decreases after 30 min until the end of the period of consideration at 44 min.

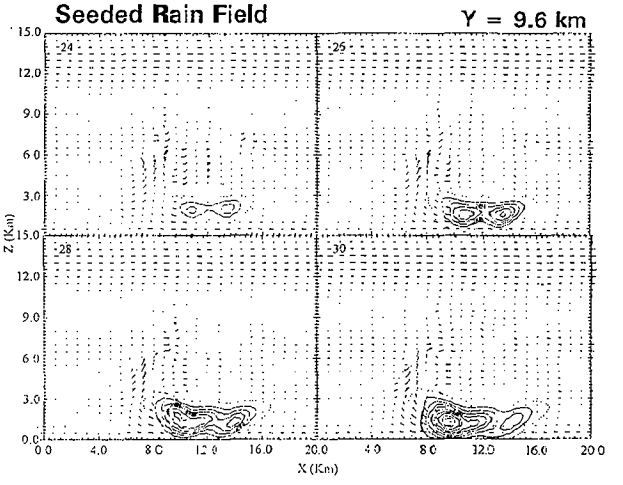

Fig. 11: X-Z cross sections of the rain field at y = 9.6 km from 24 to 30 min for the seeded case. The contour interval is 0.1 g kg^{-1} in all panels. The arrows show the wind in the X-Z plane.

Figure 12 shows X-Y cross sections of the rain field at the model surface from 30 to 36 min. At 30 min, two rain cores are clearly defined. They are much stronger than those seen in the unseeded case (Fig. 10) at the same time. The two cores merge by 32 min and grow stronger until 34 min. By 36 min, the southern portion begins to dissipate while the northern part remains fairly strong.

4. ADDITIONAL RESULTS AND GENERAL DISCUSSION

The discussion from the previous section has shown that there is a slight seeding effect in

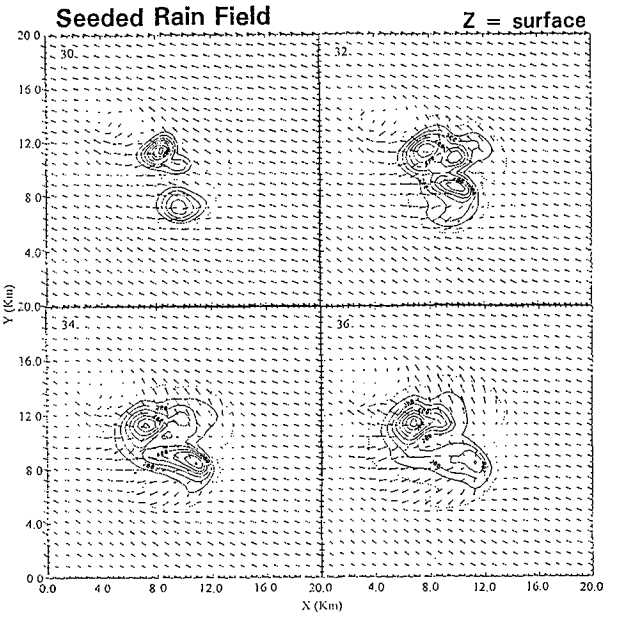

Fig. 12: X-Y cross sections of the rain field at the model surface from 30 to 36 min for the seeded case. The contour interval is 0.1 g kg^{-1} in all panels. The arrows show the wind in the X-Y plane.

the three-dimensional model results. Precipitation formation in the seeded case occurs 2 min earlier than in the unseeded case. In this section, the seeded and unseeded cases will be compared in greater detail.

Figure 13a,b illustrates the time evolution of the maximum cloud ice and snow amounts, respectively, for the two cases. Cloud ice in the seeded case shows up 2 min earlier and in larger amounts than in the unseeded case. This is a direct effect of the seeding agent. The two cases indicate the same cloud ice maximum amounts by 18 min. This occurs near the level of complete glaciation (-35°C) in the northeast quadrant. Between 20 and 30 min, the unseeded case has slightly larger maximum amounts of cloud ice than the seeded case. This is because most of the AgI has been used up by this time and the newer turret on the northwest side occurs too late for a direct seeding effect. After 30 min, the maximum cloud ice amounts in both cases slowly decrease. In terms of domain totals, the seeded case indicates an increased amount of cloud ice (5 to 10%) compared to the unseeded case after 26 min.

Figure 13b shows the time evolution of maximum amounts of snow for both cases. As expected, the snow field in the seeded case shows up 2 min earlier and in greater amounts than the unseeded case at the early stage. This is associated with the earlier formation of cloud ice shown in Fig. 13a. The two cases have almost the same maximum snow amount at 18 min, and both reach their respective highest maximum values at 24 min. There is a steady decrease after 24 min in both cases, as much of the snow is transformed into graupel. In terms of domain totals, the unseeded case indicates approximately 5% more snow than the seeded case after 24 min.

The time evolution of the maximum graupel/hail and rain mixing ratios for the two cases are illustrated in Fig. 14a,b. As was the case for cloud ice and snow, graupel/hail in the seeded case shows up 2 min earlier than in the unseeded case. The seeded case reaches its highest maximum value at 24 min, while the unseeded case does not peak until 2 min later. During this period, the maximum values remain larger in the seeded case. The rapid decrease after 26 min is due to the fallout and melting of the graupel/hail. The formation of rain in this simulation is primarily due to the melting of graupel/hail. In terms of domain totals, the seeded case indicates up to 15 KT more graupel/hail than the unseeded case from 20 to 24 min. This is equivalent to a 100% increase at 20 min, decreasing to +15% at 24 min. Both cases display steady decreases and similar values between 27 and 38 min.

Figure 14b shows that the rain field develops 2 min earlier and in larger mass concentration after 30 min in the seeded case. The rain develops later in the unseeded case, and is stronger at the later stages. In terms of domain totals, the seeded case indicates more rain (by as much as 7 KT, or +100%) out to 31 min. The values are nearly equal at 32 min, and the unseeded case indicates about 10% more rain thereafter.

Surface accumulations of rain and hail were calculated at coarse time resolution from data on the history files. These estimates indicate peak rainfall depth increased by about 5% (for values in the range of 2 mm) for the seeded case. Total rainfall was increased by over 20% in the seeded case (29 KT vs. 24 KT for the unseeded case). Hail amounts were much smaller but indicated decreases of 40% or more in the seeded case.

Figure 15 shows the time evolution of the maximum vertical velocity for the seeded and unseeded cases. This figure illustrates the single cell nature of the primary updraft which reaches its maximum value at 18 min. The decrease after 18 min is due to the loading of graupel/hail and rain. There is no evidence of a dynamic seeding effect. The secondary cell indicated in the later stages (after 36 min) is associated with new growth to the northwest of the original cell. It is of little significance to the discussion of seeding effects.

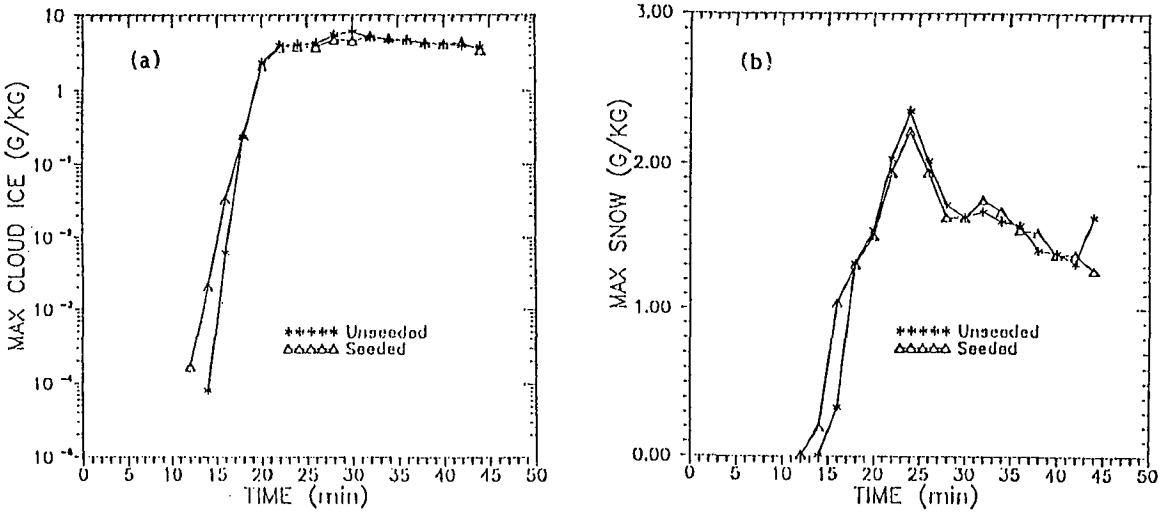

Fig. 13: (a) Time evolution of the maximum mixing ratio of cloud ice for the unseeded and seeded 3D cases. (b) Time evolution of the maximum mixing ratio of snow for the unseeded and seeded 3D cases.

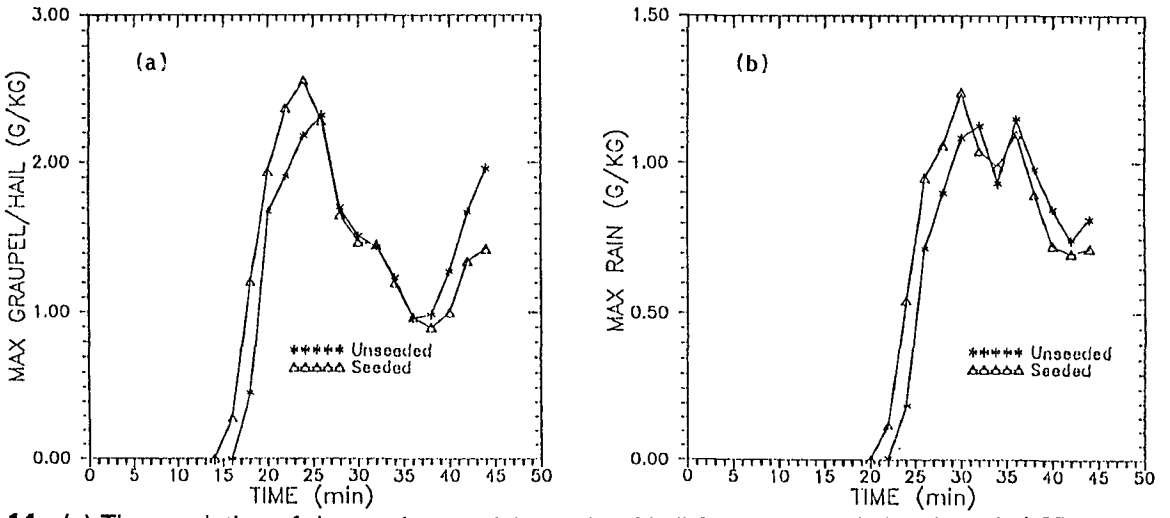

Fig. 14: (a) Time evolution of the maximum mixing ratio of hail for the unseeded and seeded 3D cases. (b) Time evolution for the maximum mixing ratio of rain for the unseeded and seeded 3D case.

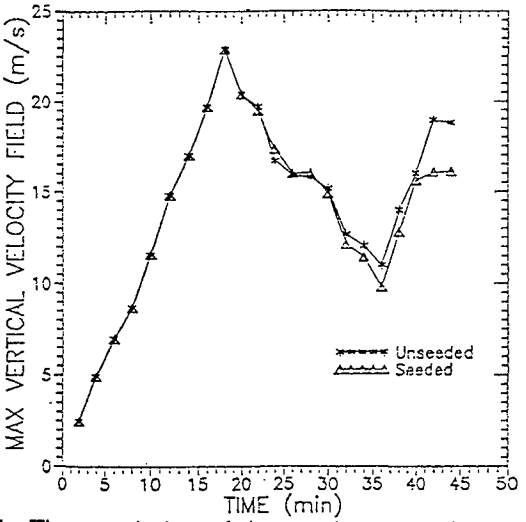

Fig. 15: Time evolution of the maximum vertical velocity for the unseeded and seeded 3D cases.

5. CONCLUSIONS

These results of cloud seeding simulations in a 3D cloud model are consistent with some of our earlier work using 2D cloud models. The earlier ice initiation caused by the seeding agent is crucial to the overall seeding effect in the model cloud, leading to increased precipitation. In this case, both seeded and unseeded model clouds develop very similarly with respect to their dynamics; not so with respect to their microphysics.

It is typical for virtually all of the AgI to be activated in 2D simulations. Seeding material transported through the sides or top of the cloud in the 2D model then tends to be drawn back into the cloud as it descends to lower levels. For the 3D seeded case in this study, 10% of the AgI remains unactivated, caught in a dead zone of virtually no net transport to the southeast of the cloud around 4 km AGL. This may be due to the less than optimal placement of the seeding agent in the three-dimensional seeded case.

It is premature at this time to make any general, sweeping conclusions about the usefulness of 2D or 3D cloud seeding results. Just because a model is 2D does not invalidate results. Just because a model is 3D does not mean that it is right. The plausibility of results from both 2D and 3D looks reasonable and supports observational results in many cases; but they both could be wrong. In addition, keep in mind that the results reported above are for one 3D cloud case only. Further work is necessary to compare 2D, 3D, and observational work to determine the usefulness and appropriateness of the models in predicting cloud seeding results.

Acknowledgments. The research was sponsored by the National Science Foundation under Grant No. ATM-9206919. Support for this computing research was provided by the National Center for Atmospheric Research, in Boulder, Colorado. The National Center for Atmospheric Research is operated by the University Corporation for Atmospheric Research and is sponsored by the National Science Foundation.

We also thank Mrs. Joie Robinson for her assistance in preparing this manuscript.

REFERENCES

Aleksić, N. M., R. D. Farley and H. D. Orville, 1989: A numerical cloud model study of the Hallet-Mossop ice multiplication process in strong convection. *Atmos. Res.*, **23**, 1-30.

Clark, T. L., 1977: A small scale numerical model using a terrain following coordinate system. *J. Comput. Phys.*, **24**, 186-215.

Clark, T. L., 1979: Numerical simulations with a three-dimensional cloud model: Lateral boundary condition experiments and multi-cellular severe storm simulations. *J. Atmos. Sci.*, **36**, 2191-2215.

Clark, T. L., 1982: Cloud modeling in three spatial dimensions, Chapter 10 in *Hailstorms of the Central High Plains*. **Vol. I**, The National Hail Research Experiment. Charles A. Knight and Patrick Squires, eds., Colorado Associated Univ. Press, Boulder, CO. 282 pp.

Clark, T. L., and R. D. Farley, 1984: Severe downslope windstorm calculations in two and three spatial dimensions using anelastic interactive grid nesting: A possible mechanism for gustiness. *J. Atmos. Sci.*, **41**, 329-350.

Dye, J. E., J. J. Jones, N. P. Winn, T. A. Cerni, B. Gardiner, D. Lamb, R. L. Pitter, J. Hallett, and C. P. R. Saunders, 1986: Early electrification and precipitation development in a small, isolated Montana cumulonimbus. *J. Geophys. Res.*, **91**, 1231-1247.

Farley, R. D., 1987: Numerical modeling of hailstorms and hailstone growth. Part III: Simulation of an Alberta hailstorm - natural and seeded cases. *J. Appl. Meteor.*, **26**, 789-812.

Farley, R. D., P. E. Price, H. D. Orville and J. H. Hirsch, 1989: On the numerical simulation of graupel/hail initiation via the riming of snow in bulk water microphysical cloud models. *J. Appl. Meteor.*, **28**, 1128-1131.

Farley, R. D., S. Wang and H. D. Orville, 1992: A comparision of 3D model results with observations for an isolated CCOPE thunderstorm. *J. Meteorol. Atmos. Phys.*, **49**, 187-207.

Helsdon, J. H., Jr., and R. D. Farley, 1987: A numerical modeling study of a Montana thunderstorm: Part I. Model results versus observations involving non-electrical aspects. *J. Geophys. Res.*, **92**, 5645-5659.

Hsie, E-Y., R. D. Farley and H. D. Orville, 1980: Numerical simulation of ice-phase convective cloud seeding. *J. Appl. Meteor.*, **19**, 950-977.

Kessler, E., 1969: On the distribution and continuity of water substance in atmospheric circulations. *Meteor. Monogr.*, **10**, No. 32. 84 pp.

Kopp, F. J., H. D. Orville, R. D. Farley and J. H. Hirsch, 1983: Numerical simulation of dry ice cloud seeding experiments. *J. Climate Appl. Meteor.*, **22**, 1542-1556.

Lilly, D. K., 1962: On the numerical simulation of buoyant convection. *Tellus*, **14**, 148-172.

Lin, Y-L., R. D. Farley and H. D. Orville, 1983: Bulk parameterization of the snow field in a cloud model. *J. Climate. Appl. Meteor.*, **22**, 1065-1092.

Nguyen, Phuong, 1993: Modeling of cloud seeding effects in one-, two-, and three-dimensional cloud models. M.S. Thesis, Dept. of Meteorology, S.D. School of Mines and Technology, Rapid City, SD. 140 pp.

Ogura, Y., and N. A. Phillips, 1962: Scale analysis of deep and shallow convection in the atmosphere. *J. Atmos. Sci.*, **19**, 173-179.

Orville, H. D., and J-M. Chen, 1982: Effects of cloud seeding, latent heat of fusion and condensate loading on cloud dynamics and precipitation evolution: A numerical study. *J. Atmos. Sci.*, **39**, 2807-2827.

Orville, H. D., R. D. Farley and J. H. Hirsch, 1984: Some surprising results from simulated seeding of stratiform-type clouds. *J. Climate Appl. Meteor.*, **23**, 1585-1600.

Smagorinsky, J., 1963: General circulation experiments with the primitive equations: 1. The basic experiment. *Mon. Wea. Rev.*, **91**, 99-164.